

Spatiotemporal Calibration of Doppler Velocity Logs for Underwater Robots

Hongxu Zhao¹, Guangyang Zeng¹, Yunling Shao¹, Tengfei Zhang¹, and Junfeng Wu¹

Abstract—The calibration of extrinsic parameters and clock offsets between sensors for high-accuracy performance in underwater SLAM systems remains insufficiently explored. Existing methods for Doppler Velocity Log (DVL) calibration are either constrained to specific sensor configurations or rely on oversimplified assumptions, and none jointly estimate translational extrinsics and time offsets. We propose a Unified Iterative Calibration (UIC) framework for general DVL–sensor setups, formulated as a Maximum A Posteriori (MAP) estimation with a Gaussian Process (GP) motion prior for high-fidelity motion interpolation. UIC alternates between efficient GP-based motion state updates and gradient-based calibration variable updates, supported by a provably statistically consistent sequential initialization scheme. The proposed UIC can be applied to IMU, cameras and other modalities as co-sensors. We release an open-source DVL–camera calibration toolbox. Beyond underwater applications, several aspects of UIC—such as the integration of GP priors for MAP-based calibration and the design of provably reliable initialization procedures—are broadly applicable to other multi-sensor calibration problems. Finally, simulations and real-world tests validate our approach.

I. INTRODUCTION

In underwater environments, traditional on-land sensors such as cameras and LiDAR face inherent limitations in perception tasks. Acoustic sensors, particularly Doppler Velocity Logs (DVLs), have become indispensable for underwater navigation and environmental sensing. To enable robust fusion of DVL measurements with data from other sensors, precise calibration of extrinsic parameters and temporal synchronization is critical, especially in challenging underwater operating conditions [1]–[5].

Prior work by Xu *et al.* [6] and Westman and Kaes [7] framed the DVL-camera calibration as an odometry alignment problem, matching the trajectory from a DVL-IMU system against the visual one from a camera. A critical limitation of these approaches is their implicit assumption of known and static DVL-IMU extrinsics, which is frequently violated in underwater environments due to their dynamic nature. While studies in [8]–[11] address the calibration of IMU-free DVLs, their applicability is strictly limited to co-sensors that provide direct linear and angular velocity measurements, such as SINS/GPS systems. Crucially, a significant gap persists across all these works: none address the calibration of translational extrinsic nor account for temporal synchronization across heterogeneous sensors. In contrast, the terrestrial robotics community has extensively investigated inter-sensor synchronization for multi-sensor

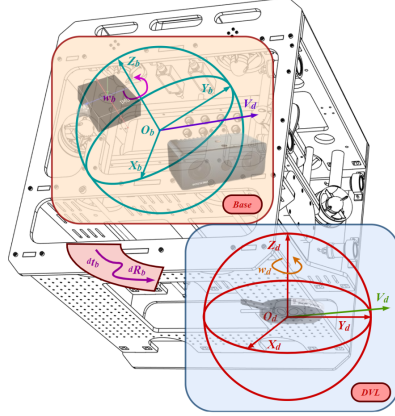


Fig. 1: DVL frame (blue) to base frame (stereo camera + IMU, orange) extrinsics.

calibration [12], [13]. State-of-the-art techniques often tackle temporal offsets by fitting continuous-time trajectories from discrete measurement points using interpolation methods, e.g., linear interpolation, B-spline fitting, or Gaussian processes (GPs).

In this paper, we aim to jointly estimate the extrinsics of the DVL frame relative to the base frame and the clock offset between them—a capability established for on-land sensor suites but largely unexplored in underwater sensing. Our formulation is general: we do not limit the DVL to being a part of DVL-IMU unit, nor the co-sensor to those providing direct velocity measurements. We propose a Unified Iterative Calibration (UIC) method to solve this problem. Our main contributions are:

- **Bayesian formulation with GP motion prior integration.** We formulate the spatiotemporal calibration problem as a Maximum A Posteriori (MAP) estimation, integrating a GP motion prior for the first time in this context. The GP prior flexibly adapts to the robot’s motion pattern, enabling high-fidelity interpolation of motion states at any instances for time synchronization.
- **An efficient MAP solver (UIC) with theoretical guarantees for robust initialization.** We propose UIC, an iterative block coordinate descent method alternating between fast GP-based motion state updates and gradient-based calibration variable updates. The state update benefits from GP regression, ensuring computational efficiency, while the calibration update is almost everywhere differentiable with respect to the time offset due to the piecewise differentiable nature of the interpolated motion. Furthermore, we prove that our sequential initialization strategy yields statistically

¹The School of Data Science, Chinese University of Hong Kong, Shenzhen, Shenzhen, P. R. China. Emails: hxxsimon99@gmail.com, zengguangyang@cuhk.edu.cn, yunlingshao@link.cuhk.edu.cn, zhantengfei@cuhk.edu.cn, junfengwu@cuhk.edu.cn.

consistent calibration estimates as measurement data accumulates.

- **Analysis of motion influence on calibration accuracy.**

We reveal that large angular velocity motions are essential for accurately estimating translation extrinsics. This theoretical finding is validated by both simulation and experimental results, and serves as a practical guideline for designing effective calibration maneuvers.

- **Open-source DVL–camera calibration toolbox.**

While our contributions are presented in the context of DVL calibration, several aspects are broadly applicable to other sensor calibration tasks. For example, GP priors provide two major benefits for motion interpolation: (i) they allow seamless fusion of asynchronous sensor measurements and prediction of motion states at arbitrary timestamps; (ii) they enable efficient refinement of time offsets by compensating motion mismatches using closed-form GP predictions. Moreover, our sequential initialization strategy is generally useful when no prior calibration knowledge is available, with reliability guaranteed theoretically.

Notation: Throughout this paper, we adhere to the following notational conventions: the super-scripted $(\cdot)^o$ represents the true value of a variable (\cdot) , (\cdot) a measurement of (\cdot) , $(\check{\cdot})$ the optimal estimate to (\cdot) under some metric, and (\cdot) an estimate to (\cdot) . For a vector $a \in \mathbb{R}^3$, let $a^\wedge \in \mathbb{R}^{3 \times 3}$ be the skew-symmetric matrix that satisfies $a \times b = a^\wedge b$ for all $b \in \mathbb{R}^3$, where \times is the vector cross product. The notation $X = O_p(a)$ means that the set of values X/a is stochastically bounded, and $X = o_p(a)$ means that the set of values X/a converges to zeros in probability.

II. RELATED WORK

Spatial and temporal calibrations are reviewed separately in sequence.

For DVLs equipped with integrated IMUs, Westman *et al.* [7] proposed a factor-graph optimization framework to fuse data from DVLs and cameras. Their method utilizes an AprilTag calibration board to achieve precise, drift-free pose estimation of the underwater robot, thereby enabling extrinsic calibration between the camera and the DVL’s odometry frame. Building on a similar optimization-based approach, Xu *et al.* [6] introduced a visual-acoustic bundle adjustment system within a graph SLAM framework for jointly calibrating a DVL and a camera. A key advantage of their approach is the elimination of pre-set marker panels through the use of visual environment features. In contrast, existing methods for calibrating IMU-free, standalone DVLs focus on their integration with other navigation systems. For instance, Xu and Guo [8] developed a calibration algorithm for a DVL paired with a SINS/GPS system that provides high-precision velocity references. Their method first calculates the velocity scale factor by comparing the velocity norms from the DVL and the SINS/GPS, then estimates the relative rotation using an iterated extended Kalman filter (IEKF) [9].

Temporal calibration is critical for achieving clock synchronization at the software level in low-cost or custom-assembled multi-sensor systems. To the best of our knowl-

edge, no temporal calibration results have been reported for DVLs; therefore, we review only the results for other types of sensors. Early work by Furgale *et al.* [14] introduced a B-spline-based method to transform discrete sensor measurements into continuous-time trajectories, facilitating robust estimation of inter-sensor time offsets. Li and Mourikis later proposed an extended Kalman filter (EKF) framework for joint spatiotemporal calibration, simultaneously addressing both temporal and spatial misalignments. Subsequent research emphasized efficiency and practicality. Qin and Shen [12] presented the first online temporal calibration method for camera–IMU systems. Instead of shifting sensor timelines, they adjusted feature positions within image frames under a constant-velocity motion prior—a strategy that significantly reduced computational complexity without sacrificing accuracy. Peri *et al.* [15] offered a different take on motion priors, employing a GP with a constant-acceleration assumption to represent continuous-time trajectories, thereby enabling a probabilistic and uncertainty characterization.

III. PROBLEM FORMULATION

A. DVL Measurement Model

When a DVL is mounted on an underwater robot, it emits acoustic beams and measures the Doppler shifts resulting from the robot’s movement to its ambient environment, which enables the DVL to calculate a three-dimensional velocity under the assumption of a constant and known acoustic speed.

Mathematically, DVL measurements are resolved relative to its local body-fixed frame $\{\mathcal{F}_d\}$. To analyze the motion of DVL with respect to a base frame $\{\mathcal{F}_b\}$, usually attached to the other sensor, to which the DVL is calibrated, let $p_{o_d, b}$ denote the coordinates of the origin o_d of $\{\mathcal{F}_d\}$ in frame $\{\mathcal{F}_b\}$. Essentially, the DVL measures the line velocity v_d of o_d with respect to its own frame $\{\mathcal{F}_d\}$. Provided that the base frame and the DVL frame are rigidly connected, when the base frame moves with a linear velocity v_b and angular velocity ω_b with respect to $\{\mathcal{F}_b\}$, the relationship between v_d and (v_b, ω_b) is shown as follows:

$$v_d = {}^d R_b (v_b + \omega_b \times {}^d t_b), \quad (1)$$

where ${}^d R_b \in \mathbb{R}^3$ and ${}^d t_b \in \mathbb{R}^3$ are the rotation and translation from the base frame $\{\mathcal{F}_b\}$ to the local DVL frame $\{\mathcal{F}_d\}$, respectively.

To account for real-world factors, the DVL model includes a scaling factor κ_d , representing the ratio between the real sound velocity and the nominal one, and an additive measurement noise term. Hence, a real DVL measurement \check{v}_d can be modeled as

$$\check{v}_d = \kappa_d {}^d R_b (v_b + \omega_b \times {}^d t_b) + n_v, \quad (2)$$

where $n_v \sim \mathcal{N}(0, Q_d)$ denotes the measurement noise which can be given by DVL sensor.

B. Unified Spatiotemporal Calibration Problem under GP Motion Prior

The robot motion, i.e., the evolution of the robot poses and velocities, relative to a fixed world frame can be described by a state-space Gaussian process (GP), i.e.,

$$X(T) \sim \mathcal{GP}(\mu(T), K(T, T')), \quad (3)$$

where K is the GP kernel and $X(T)$ is vector function. States can be observed from the DVL frame $\{\mathcal{F}_d\}$ over time ${}^d T$ and referenced to the base frame $\{\mathcal{F}_b\}$ and base time ${}^b T$. The GP kernel is assumed to be known, having been identified a priori through a system identification. The j -th measurement \dot{m}_j on base frame can be described as

$$\dot{m}_{b,j} = h(X({}^b T_j)) + n_j, \quad n_j \sim \mathcal{N}(0, R_i), \quad j \in [1 \dots M]. \quad (4)$$

Let $\dot{M}_b = [\dot{m}_{b,1} \dots \dot{m}_{b,M}]^\top$ and H be the Jacobian of $h(\cdot)$. In addition to the spatial transformation between $\{\mathcal{F}_d\}$ and $\{\mathcal{F}_b\}$, a clock offset may also exist between them, termed ${}^b \delta_{T,d}$. It is assumed to be fixed within the calibration period and defined as

$${}^b \delta_{T,d} = {}^b T_k - {}^d T_k, \quad \forall k \in \{1, \dots, K\},$$

where ${}^b T_k$ and ${}^d T_k$ denote the timestamp of some event k recorded by the base system and DVL system, respectively. The focus of this paper is on the unified spatiotemporal calibration of the transformation $({}^d R_b, {}^d t_b)$, the clock offset ${}^b \delta_{T,d}$ and the velocity scaling factor κ_d , to be estimated jointly from the robot's motion.

Let $X_b = (X_{b,j})_{j=1}^M$ denote the base frame's motion states at the instants of sensor measurements attached to the base, and let $X_d = (X_{d,i})_{i=1}^N$ denote the motion states of the DVL frame at the instants of DVL measurements. The timestamps of these events are recorded in the order in accordance with the sequences X_b and X_d according to their respective clocks, and define two sets: ${}^b T = ({}^b T_j)_{j=1}^M$ and ${}^d T = ({}^d T_i)_{i=1}^N$. Let $X = [X_{b,1}^\top \dots X_{b,M}^\top, X_{d,1}^\top \dots X_{d,M}^\top]^\top$. Define the term $J_{\text{GP}}(X, {}^b \delta_{T,d})$ is the costs associated with GP prior factors, which writes

$$J_{\text{GP}}(X, {}^b \delta_{T,d}) = r_{\text{GP}}^\top K^{-1} r_{\text{GP}}, \quad (5)$$

where

$$r_{\text{GP}} = X - \mu, \quad \mu = \begin{bmatrix} \mu({}^b T_1) \\ \vdots \\ \mu({}^b T_M) \\ \mu({}^d T_1 + {}^b \delta_{T,d}) \\ \vdots \\ \mu({}^d T_N + {}^b \delta_{T,d}) \end{bmatrix} = \begin{bmatrix} \mu_1 \\ \mu_2({}^b \delta_{T,d}) \end{bmatrix} \quad (6)$$

and $K = \begin{bmatrix} K_1 & K_2({}^b \delta_{T,d}) \\ K_3({}^b \delta_{T,d}) & K_4({}^b \delta_{T,d}) \end{bmatrix}$ is given by

$$\begin{bmatrix} K({}^b T_1, {}^b T_1) & \dots & K({}^b T_1, {}^d T_N + {}^b \delta_{T,d}) \\ \vdots & \ddots & \vdots \\ K({}^d T_N + {}^b \delta_{T,d}, {}^b T_1) & \dots & K({}^d T_N + {}^b \delta_{T,d}, {}^d T_N + {}^b \delta_{T,d}) \end{bmatrix}.$$

Define the term $J_{b,\text{M}}(X_b)$ that aggregates the costs from the base measurements against a prediction from given

model, which has the form $J_{b,\text{M}}(X_b) = \dot{M}_b - h(X({}^b T))$. Define the term $J_{d,\text{M}}(X_d, {}^d R_b, {}^d t_b, \kappa_d)$ as the cost resulted from the DVL measurements, which writes

$$J_{d,\text{M}}(X_d, {}^d R_b, {}^d t_b, \kappa_d) = \sum_{i=1}^N \| \dot{v}_{d,i} - \kappa_d {}^d R_b (v_{b,i} + \omega_{b,i} \times {}^d t_b) \|_{Q_d}^2,$$

where $v_{b,i}, \omega_{b,i} \in X_{d,i}$. Finally, we arrive at a joint optimization problem over the motion states and the calibration parameters of interest,

$$\begin{aligned} \min_{{}^b \delta_{T,d}, {}^d R_b, {}^d t_b, \kappa_d, X} & J_{\text{GP}}(X, {}^b \delta_{T,d}) + J_{b,\text{M}}(X_b) + J_{d,\text{M}}(X_d, {}^d R_b, {}^d t_b, \kappa_d) \\ \text{s.t.} & {}^d R_b \in \text{SO}(3), \quad {}^d t_b \in \mathbb{R}^3, \quad \kappa_d > 0. \end{aligned} \quad (7)$$

In the problem, $J_{b,\text{M}}(X_b) + J_{d,\text{M}}(X_d, {}^d R_b, {}^d t_b, \kappa_d)$ are the log-likelihoods derived from the base and DVL measurements, penalizing prediction errors, while $J_{\text{GP}}(X, {}^b \delta_{T,d})$ is a prior that enforces GP motion smoothness between states offset by ${}^b \delta_{T,d}$. This formulation is a maximum a posteriori (MAP) estimation problem for unified spatiotemporal calibration, with X treated as latent variables, which is the first Bayesian interpretation of calibration problem. The problem is highly nonlinear, so we temper our expectations of obtaining a globally optimal solution. Instead, in what follows, we develop a block coordinate descent (BCD) approach, referred to as the Unified Iterative Calibration (UIC) method.

IV. METHODOLOGY

The UIC algorithm, in the spirit of the BCD approach, tackles problem (7) by grouping X into one block and the calibration parameters into another, and then solving a smaller problem for each block while keeping the other fixed, iterating until convergence is achieved or some termination condition is met. In what follows, we discuss the block variable initialization and present the UIC iteration process in detail.

A. Sequential Initialization Strategy

Our initialization procedure separates the motion state X from the calibration parameters ${}^d R_b$, ${}^d t_b$, κ_d , and ${}^b \delta_{T,d}$. Concretely, UIC first estimates the base and DVL trajectories, X_b and X_d , via GP regression involving only two factors: the GP prior $J_{\text{GP}}(X)$ and the base measurement factor $J_{b,\text{M}}(X_b)$. The DVL measurement factor $J_{d,\text{M}}(X_d, {}^d R_b)$ is excluded at this stage—thereby losing some refinement from DVL measurements—in order to estimate X in a straightforward manner using the linear prediction equations (10), rather than smoothing conditioned on DVL measurements.

The sequential strategy is motivated by the expectation that it yields a stable initial estimate of X and, subsequently, a good initialization of the calibration parameters, for two reasons: First, the resulting GP regression problem can be efficiently and accurately solved by filtering techniques from SLAM [16] or by state-of-the-art graph optimization solvers [17]. Second, as will be shown in Theorems 1 and 2, the estimate \hat{X} is asymptotic unbiased under some technical

conditions—a property that is highly desirable for initializing the calibration variables.

Directly optimizing Equation (7) from random initialization offers no strong convergence guarantees. The objective is highly nonconvex and sensitive to the initial values of the calibration variables; poor initial guesses often lead to divergence or convergence to suboptimal local minima. In our experiments, naive initialization frequently resulted in non-convergence. The initialization procedures for X and the calibration parameters are presented in the next two subsections.

B. Initialization of Motion State X

By virtue of sequential initialization, an estimate \hat{X} of X is obtained as

$$\hat{X} = \arg \min_{X_b, X_d} J_{\text{GP}}(X, {}^b\delta_{T,d}) + J_{b,\text{M}}(X_b), \quad (8)$$

which admits a closed-form solution as a function ${}^b\delta_{T,d}$. According to the linear prediction equations [18, (50)], the structure of \hat{X}_b is as follows: first, \hat{X}_b is estimated via GP regression as

$$\hat{X}_b = \mu_1 + K_1 H^\top (R + H K_1 H^\top)^{-1} (M_b - H \mu_1). \quad (9)$$

then \hat{X}_d is computed as a linear combination of \hat{X}_b , with weights determined explicitly by bT , dT and ${}^b\delta_{T,d}$, i.e.,

$$\hat{X}_d({}^b\delta_{T,d}) = \mu_2({}^b\delta_{T,d}) - K_3({}^b\delta_{T,d}) K_1^{-1}(\mu_1 - \hat{X}_b). \quad (10)$$

which \hat{X}_d is clearly expressed as a function of ${}^b\delta_{T,d}$. Note that (8) can be solved using graph-based optimization for a general kernel K GTsam or Ceres; or alternatively, if the GP kernel admits a Markov state-space representation, it can be efficiently with a Kalman filter, such as InEKF. In addition, according to [19], the uncertainty of the posterior distribution can be characterized as a byproduct of GP regression, given as

$$\begin{aligned} \Sigma_{X_b} &= K_1 - K_1 H^\top (R + H K_1 H^\top)^{-1} H K_1, \\ \Sigma_{X_d}({}^b\delta_{T,d}) &= K_4({}^b\delta_{T,d}) - \\ &\quad K_3({}^b\delta_{T,d}) K_1^{-1}(K_1 - \Sigma_{X_b}) K_1^{-1} K_2({}^b\delta_{T,d}). \end{aligned} \quad (11)$$

C. Initialization of Calibration Variables

We next initialize the calibration variables using all DVL measurements together with the GP estimate $\hat{X}_d({}^b\delta_{T,d})$. Specifically, we can solve

$$\min_{{}^dR_b, {}^d t_b, \kappa_d, {}^b\delta_{T,d}} J_{d,\text{M}}(\hat{X}_d({}^b\delta_{T,d}), {}^dR_b, {}^d t_b, \kappa_d). \quad (12)$$

This formulation is an error-in-variables problem in estimation theory [20], since $\hat{X}_d({}^b\delta_{T,d})$ constitutes another set of random variables that is independent of the DVL measurement noise. While (12) can, in principle, be solved using a nonlinear programming solver, ensuring convergence and calibration accuracy remains challenging. Moreover, even a globally optimal solution to this problem is not necessarily unbiased [21], [22].

To mitigate these difficulties, we decouple the calibration of the extrinsic parameters dR_b and ${}^d t_b$ from that of the temporal offset and scale parameters ${}^b\delta_{T,d}$ and κ_d by leveraging specialized robot motion patterns. As will be shown shortly, the resulting separate estimators can be computed efficiently—via line-search-bootstrapped iterative gradient descent for the temporal/scale parameters, and a closed-form solution for the spatial extrinsics—and are guaranteed to asymptotically converge to the true calibration values at a rate of at a rate of $1/\sqrt{N_D}$, where N_D denotes the number of DVL measurements.

1) *Consistent clock offset estimator*: In principle, we will estimate the clock offset ${}^b\delta_{T,d}$ by maximizing the alignment between the DVL measurements and the predicted DVL output based on $\hat{X}_d({}^b\delta_{T,d})$. Specifically, the predicted DVL velocity is given by

$$\kappa_d {}^dR_b (\hat{v}_{b,i}({}^b\delta_{T,d}) + \hat{w}_{b,i}({}^b\delta_{T,d}) \times {}^d t_b), \quad (13)$$

according to (2). To eliminate the influence of the spatial extrinsics, we select measurement data, forming a set \mathcal{D}_o , with small angular velocity, i.e., $\omega_{b,i} \approx 0$. Under this condition, the lever-arm term $\omega_{b,i}({}^b\delta_{T,d}) \times {}^d t_b$ becomes negligible. Furthermore, taking the Euclidean norm of ${}^dR_b v_b$ in (2) removes the effect of dR_b , as the Euclidean norm is rotation-invariant. Combining these yields

$$\begin{aligned} \|\hat{v}_d({}^b\delta_{T,d})\|^2 &\approx \|{}^dR_b(v_b^o + n_{v_b}(\delta))\|^2 \\ &= \|v_b^o\|^2 + 2v_b^o{}^\top n_{v_b}(\delta) + \|n_{v_b}(\delta)\|^2, \end{aligned} \quad (14)$$

where $n_{v_b}(\delta)$ is the noise capturing the randomness contained in $\hat{v}_d({}^b\delta_{T,d})$, which is unbiased due to GP regression and its variance is $\Sigma_{X_d}({}^b\delta_{T,d})$ given in (11), and

$$\begin{aligned} \|\hat{v}_{d,i}\|^2 &= \|\kappa_d^o v_d^o + n_{v,i}\|^2, \quad i \in \mathcal{D}_o \\ &= \kappa_d^{o2}(\|v_d^o\|^2 + v_d^o{}^\top n_{v,i} + \|n_{v,i}\|^2). \end{aligned}$$

We substitute $\|v_d^o\|^2$ in the above equation with $\|\hat{v}_d({}^b\delta_{T,d})\|^2$ according to the relation (14) and shift the mean of the noise terms to zero, we obtain the following optimization problem over a two-dimensional search space:

$$\min_{{}^b\delta_{T,d}, \kappa_d} \left(\frac{\|\hat{v}_{d,i}\|^2}{\kappa_d^2} - \|\hat{v}_d({}^b\delta_{T,d})\|^2 + \text{tr}(\Sigma_v({}^b\delta_{T,d})) - \frac{\text{tr}(Q_d)^2}{\kappa_d^2} \right)^2. \quad (15)$$

Since κ_d^o is practically very close to 1, the problem can be efficiently solved by performing a line search over ${}^b\delta_{T,d}$ while varying κ_d^o over a small grid around 1. Let ${}^b\hat{\delta}_{T,d}$ and $\hat{\kappa}_d$ be the global optimum. The following result claims the consistency of ${}^b\hat{\delta}_{T,d}$ and $\hat{\kappa}_d$ under ideal condition $\omega_{b,i} = 0$ for $i \in \mathcal{D}_o$.

Theorem 1: ${}^b\hat{\delta}_{T,d}$ and $\hat{\kappa}_d$ are \sqrt{N} -consistent estimates of ${}^b\delta_{T,d}^o$ and κ_d^o .

2) *Consistent extrinsics estimator*: Stacking all DVL measurements as $\hat{V}_d = [\hat{v}_{d,1} \cdots \hat{v}_{d,N}]^\top$, we arrive at the stacked version of (2):

$$\hat{V}_d = \kappa_d V_b^{od} R_b^\top - \kappa_d \Omega_b^{od} ({}^d t_b)^\top {}^d R_b^\top + N_v, \quad (16)$$

where $V_b^o = [v_{b,1}^o \cdots v_{b,N}^o]^\top$, $\Omega_b^o = [\omega_{b,1}^o \cdots \omega_{b,N}^o]^\top$ and $N_v = [n_{v,1} \cdots n_{v,N}]^\top$. Define $Z = [Z_1 \ Z_2]^\top$, where

$Z_1 = \kappa_d {}^d R_b$ and $Z_2 = \kappa_d {}^d R_b ({}^d t_b)^\wedge$, and $H^o = [V_b^o - \Omega_b^o]$. Then (16) is written as $\mathring{V}_d = H^o Z + N_v$. Omitting the $SO(3)$ constraint of ${}^d R_b$, We estimate Z by solving

$$\operatorname{argmin}_Z \|\mathring{V}_d - H^o Z\|_F^2,$$

which admits the closed-form solution

$$\hat{Z} = \left(\frac{H^{o\top} H^o}{N} \right)^{-1} \left(\frac{H^{o\top} \mathring{V}_d}{N} \right). \quad (17)$$

We note that κ_d is estimated again in the above problem. This is a deliberate technical choice: the earlier estimation used only a selected subset \mathcal{D}_o of DVL measurements with $\omega_{b,i} \approx 0$, which represents a relatively limited volume of data. In contrast, the stacked formulation (16) uses the entire measurement set. By Remark 1, this yields a more reliable estimate of κ_d in the sense that it exhibits less variance around the true value.

The exact values of $v_{b,i}^o$ and $\omega_{b,i}^o$ are not directly measurable, therefore their estimates $\hat{v}_{b,i}$ and $\hat{\omega}_{b,i}$ from \hat{X}_b are substituted into (17). Accordingly, \hat{Z} should be corrected via bias elimination to account for this substitution. The resulting estimate is

$$\hat{Z}^c = \left(\frac{\hat{H}^\top \hat{H} - G}{N} \right)^{-1} \left(\frac{\hat{H}^\top \mathring{V}_d}{N} \right), \quad (18)$$

where $\hat{H} = [\hat{V}_b - \hat{\Omega}_b]$ with $\hat{V}_b = [\hat{v}_{b,1}({}^b \hat{\delta}_{T,d}) \cdots \hat{v}_{b,N}({}^b \hat{\delta}_{T,d})]$ and $\hat{\Omega}_b = [\hat{\omega}_{b,1}({}^b \hat{\delta}_{T,d}) \cdots \hat{\omega}_{b,N}({}^b \hat{\delta}_{T,d})]$ and G is the submatrix corresponding to the v_b and ω_b components. We further reconstruct $\hat{\kappa}_d^c$ from \hat{Z}^c as

$$\hat{\kappa}_d^c = |\det^{1/3}(\hat{Z}_1^c)|, \quad (19)$$

which follows from $\det({}^d \hat{R}_b^o) = 1$. Performing singular value decomposition (SVD) to $\hat{Z}_1^c / \hat{\kappa}_d^c$, we set ${}^d \hat{R}_x$, denoted as $U_R \Sigma_R V_R^\top$, then set

$${}^d \hat{R}_X^c = U_R \operatorname{diag}([1, 1, \det(U_R V_R^\top)]) V_R^\top. \quad (20)$$

We then recover an estimate ${}^d \hat{t}_b^{i\wedge}$ from \hat{Z}_2^c as

$${}^d \hat{t}_b^{c\wedge} = ({}^d \hat{R}_X^{c\top} \hat{Z}_2^c / \hat{\kappa}_d^c - ({}^d \hat{R}_X^{c\top} \hat{Z}_2^c / \hat{\kappa}_d^c)^\top) / 2. \quad (21)$$

The following result asserts the consistency the these structured estimates.

Theorem 2: ${}^d \hat{R}_b^c$, $\hat{\kappa}_d^c$, and ${}^d \hat{t}_b^c$ are \sqrt{N} -consistent estimates of ${}^d R_b^o$ and κ_d^o and ${}^d t_b^o$.

The proof for both theorems are similar in [23].

D. The Whole Algorithm

The whole UIC algorithm is summarized as follows. First, an intial values for X , ${}^d R_b$, ${}^d t_b$, κ_d , ${}^b \delta_{T,d}$ are obtained following the procedures described in Sections IV-B and IV-C. An iterative loop is then executed: in each iteration, the extrinsic variables are fixed to the values from the previous iteration, and the motion state X is updated—either exactly or approximately (in this work, the update is performed in exact form via complete GP regression). Next, the extrinsic parameters are updated on top of the improved states. These two steps alternate until the stopping criterion is met. Standard

Algorithm 1 UIC for DVL Spatiotemporal Calibration

Input: local time-stamped DVL measurements \mathring{V}_d 's; local time-stamped base measurements \mathring{m}_b 's; GP kernel K ; stop criterion
Output: \hat{X} ; ${}^d \hat{R}_b$, ${}^d \hat{t}_b$, $\hat{\kappa}_d$, ${}^b \hat{\delta}_{T,d}$

- 1: Initialize $\hat{X}^{(0)}$, ${}^d \hat{R}_b^{(0)}$, ${}^d \hat{t}_b^{(0)}$, $\hat{\kappa}_d^{(0)}$, ${}^b \hat{\delta}_{T,d}^{(0)}$ from Algorithm 2.
- 2: **repeat**
- 3: **State update:** Compute $\hat{X}^{(k)}$ from solving (7) (GP regression) with fixed calib. vars from iteration $k-1$.
- 4: **Calibration update:** ${}^d \hat{R}_b^{(k)}$, ${}^d \hat{t}_b^{(k)}$, $\hat{\kappa}_d^{(k)}$, ${}^b \hat{\delta}_{T,d}^{(k)}$ \leftarrow gradient descent on (7) with fixed $\hat{X}^{(k)}$.
- 5: $k \leftarrow k + 1$.
- 6: **until** stop criterion is met.

stopping criteria include: a sufficiently small change in the optimization variables or in the objective value, or reaching a predefined maximum number of iterations. Robustness-aware losses can be further incorporated to improve resilience to outliers. In calibration practice, the alternating refinement converges rapidly to stable, high-accuracy solutions. The complete UIC procedure is summarized in Algorithm 1.

Remark 1: To improve the accuracy of the calibration parameters in Equation (12), we expect as many measurements as practicable, spanning diverse motion and, in particular, segments with strong angular-velocity excitation. Larger datasets generally yield more stable and reliable solutions, while rich rotational excitation improves the observability and thus the accuracy of the lever arm ${}^d t_b$.

Algorithm 2 UIC Initialization

Input: local time-stamped DVL measurements \mathring{V}_d 's; local time-stamped base measurements \mathring{m}_b 's; GP kernel K

Output: \hat{X}_{init} ; ${}^d \hat{R}_{b,\text{init}}$, ${}^d \hat{t}_{b,\text{init}}$, $\hat{\kappa}_{d,\text{init}}$, ${}^b \hat{\delta}_{T,d,\text{init}}$

- 1: Compute $\hat{X}_{b,\text{init}}$ and $\hat{X}_{d,\text{init}}$ via (9) and (10) using \mathring{m}_b and K .
- 2: Substitute $\hat{X}_{d,\text{init}}$ and \mathring{V}_d 's into (15); perform line search for initial κ_d , ${}^b \delta_{T,d,\text{init}}$ in (15); execute gradient descent iteratively to obtain $\hat{\kappa}_d$, ${}^b \hat{\delta}_{T,d}$.
- 3: Compute $\hat{\kappa}_{d,\text{init}}$, ${}^d \hat{R}_{b,\text{init}}$ and ${}^d \hat{t}_{b,\text{init}}$ via (19), (20) and (21) using ${}^b \hat{\delta}_{T,d}$ and \hat{X}_d , \mathring{V}_d .

V. NUMERICAL ANALYSIS

In this section, we perform numerical simulations to evaluate the properties and performance of our proposed UIC initialization algorithm. To the best of our knowledge, no prior work has fully addressed the spatiotemporal calibration of κ_d , ${}^d R_b$, ${}^d t_b$, and ${}^b \delta_{T,d}$ for DVL. In the simulation, the DVL velocity measurement noise is set to be with a variance of $\sigma_v^2 = 10^{-4}$ (m/s)² per axis, which is consistent with typical real DVL variances on the order of 10^{-5} – 10^{-4} (m/s)².

We synthesize trajectories and states by sampling from a GP prior induced by the white-noise-on-jerk (WNOJ) model [24]. To simulate posterior uncertainty from GP regression, we add independent zero-mean Gaussian perturba-

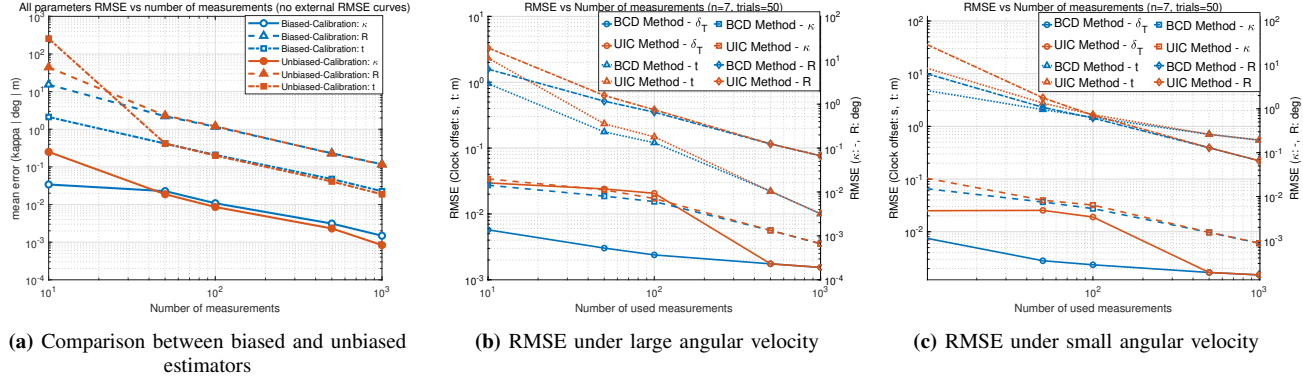


Fig. 2: Simulation results: (a) validates of the effect of bias elimination, (b) and (c) show the performances of two methods, BCD with a good initial value and the UIC initialization method, under large and small angular velocity excitations.

tions to each state. The GP kernel is set as a diagonal output-scale matrix $\text{diag}([500, 500, 500, 5, 5, 5])$. The standard deviations for the injected perturbations for 6×1 components of states are $\text{diag}([0.05, 0.02, 0.05, 0.02, 0.05, 0.02])$. Each trajectory lasts for 100 seconds, with DVL frequency of 10Hz and base state measurement frequency 10Hz. We design two simulations to validate: 1) the effect of bias elimination; 2) the performance of our UIC algorithm under different situations.

A. Effect of bias elimination

We set the clock offset to 0 seconds and compare the performance of our bias-eliminated estimator (18) with the biased estimator (17). From Fig. 2(a), our unbiased estimator outperforms the biased estimator as the number of measurements increases, while the biased estimator has better performance in a small number of measurements. In most calibration scenarios, the measurement number is usually large. Therefore, our unbiased estimator will have better accuracy than the biased estimator in practical calibration missions.

B. Performance under different excitation conditions

To enable clock-offset estimation, each trajectory is designed with two phases: the first half exhibits low rotational excitation by setting the GP kernel to $\text{diag}([500, 500, 500, 10^{-10}, 10^{-10}, 10^{-10}])$, while the second half contains strong rotational motion. We fix the clock offset as 0.07s and vary the number of measurements $N = 10, 50, 100, 500, 1000$. In addition, instead of exciting strong rotations in the second half, we also test the motion trajectory throughout which we maintain small rotational motion to analyze the performance under small angular velocity excitation. Results are plotted in Figs. 2(b) and 2(b), where UIC method denotes our UIC initialization solution and BCD method indicates the BCD method with random initialization around the true value. When there is enough rotational excitation, from Fig. 2(b), the BCD method initially outperforms the UIC method; however, once the measurement count reaches about 500, both methods converge to the same performance. This demonstrates the

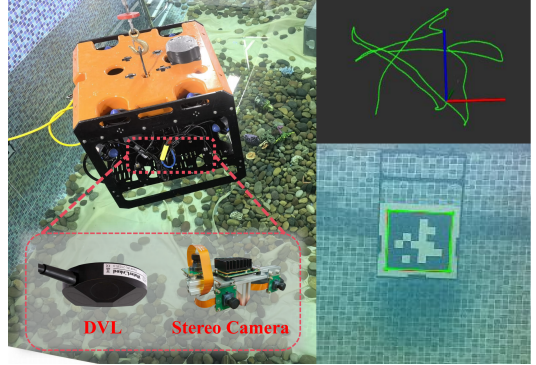


Fig. 3: Water pool experiments. Left: Underwater robot; bottom right: AprilTag board; upper right: robot trajectory.

high accuracy of our consistent UIC initialization estimator, which serves as an excellent initial value and requires only a few subsequent BCD iterations to achieve convergence. Under low excitation conditions, as shown in Fig. 2(c), the translation (lever-arm) parameter ${}^d t_b$ performs around two orders of magnitude worse than in the previous setting. This underscores that without sufficient angular velocity excitation, it is inherently impossible to reliably recover ${}^d t_b$, as discussed in Remark 1.

VI. REAL-WORLD EXPERIMENT

We conducted a real-world experiment to evaluate our calibration method. We recorded our calibration trajectories in a $4.5 \times 10 \times 2$ m pool. An A50 DVL (around 10 Hz) is mounted on an underwater robot together with a forward-looking stereo camera (10Hz). Fig. 3 shows the setting of our experiment. The stereo camera provides absolute pose measurements by observing an AprilTag board affixed to the pool wall. We calibrate the camera-DVL extrinsics ${}^d R_c, {}^d t_c$, their clock offset ${}^c \delta_{T,d}$, and the DVL scale factor κ_d .

We apply GP with WNOJ prior to estimate trajectories and manually set the kernel Q_c as $\text{diag}([100, 100, 100, 100, 100, 100])$. To evaluate the calibration performance, we construct an odometry that integrates the DVL linear velocity measurements with

TABLE I: ATE and RPE results across methods and trajectories. **Blue in bold** marks the best performance, and **light blue** marks the second-best. Our UIC method is used as the baseline; percentages indicate performance relative to UIC.

Calibration		Traj A				Traj B				Traj C				Average	
Evaluate		Traj B		Traj C		Traj A		Traj C		Traj A		Traj B		Comparison	
Method	Result	ATE	RPE												
UIC	Meter	0.348	0.107	0.621	0.156	0.151	0.070	0.538	0.141	0.209	0.067	0.230	0.071	0.350	0.091
BCD	Meter	0.368	0.107	0.606	0.154	0.166	0.070	0.529	0.142	0.231	0.070	0.237	0.072	0.356	0.105
(init. 1)	%	105.7	100	97.66	98.72	109.9	100	98.3	100.30	110.5	104.5	103.0	101.4	101.7	115.4
BCD	Meter	0.367	0.107	0.993	0.144	1.259	0.201	0.942	0.138	1.158	0.196	0.750	0.102	0.912	0.148
(init. 2)	%	105.5	100	159.9	92.31	833.0	286.3	175.1	97.4	554.1	292.5	326.1	143.7	260.6	162.6
Manual	Meter	0.378	0.108	0.621	0.158	0.262	0.085	0.607	0.157	0.262	0.085	0.390	0.109	0.420	0.117
(w. δ_T)	%	108.6	100.9	100	101.3	173.2	120.8	112.7	111.1	125.8	128.4	169.6	153.5	120	128.6
Manual	Meter	0.388	0.108	0.632	0.158	0.248	0.088	0.632	0.158	0.248	0.088	0.388	0.108	0.423	0.118
(w.o. δ_T)	%	111.5	100.9	101.8	101.3	164.2	124.7	117.5	111.8	118.7	128.4	168.7	152.1	120.9	129.7

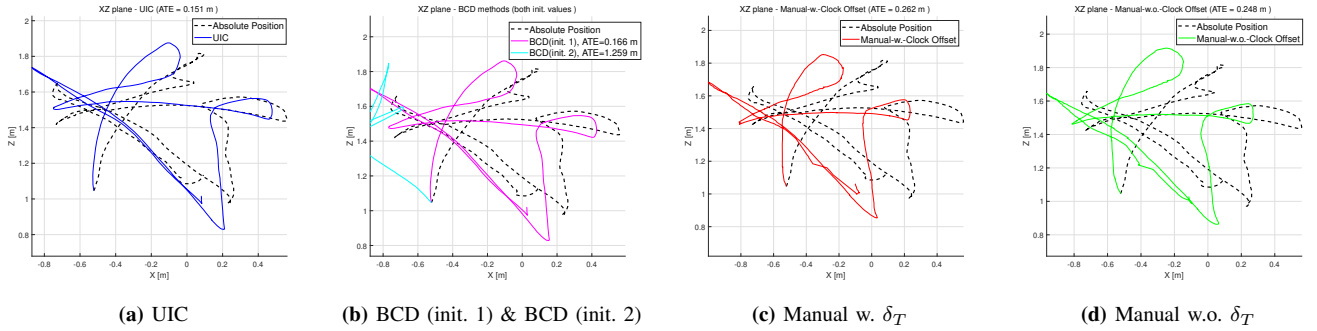


Fig. 4: Trajectory A estimation using the parameters calibrated from trajectory B.

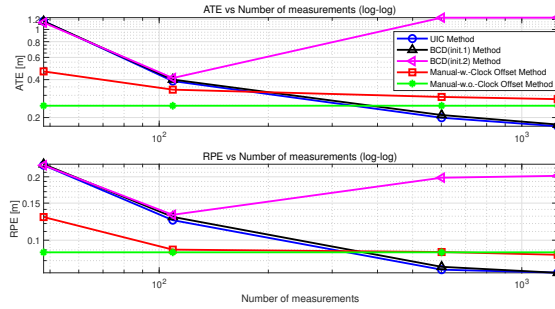


Fig. 5: Performance of different methods with respect to the measurement number.

the stereo camera's absolute orientation measurements as follows. Let ${}^wR_c(T_c)$ denote the camera orientation in the world frame at time T_c . Over a short interval $[T_{c,1}, T_{c,2}]$ between two camera measurements, since the DVL has the same frequency as the camera, there exist two DVL measurements $\dot{v}_{d,1}$ and $\dot{v}_{d,2}$ at times $T_{d,1} + {}^c\delta_{T,d}$ and $T_{d,2} + {}^c\delta_{T,d}$, which satisfy $T_{d,1} + {}^c\delta_{T,d} \leq T_{c,1}$ and $T_{d,2} + {}^c\delta_{T,d} \in [T_{c,1}, T_{c,2}]$. Then, the average velocity in this interval can be approximated by $v_d = \frac{\dot{T}_{d,2} + {}^c\delta_{T,d} - T_{c,1}}{\Delta_T} \dot{v}_{d,1} + \frac{T_{c,2} - \dot{T}_{d,2} - {}^c\delta_{T,d}}{\Delta_T} \dot{v}_{d,2}$, where $\Delta_T = T_{c,2} - T_{c,1}$. Finally, the world-frame camera position update over this interval is approximated by ${}^w p_2 \approx {}^w p_1 + \kappa_d^{-1} {}^w R_c(T_{c,1}) {}^c R_d v_d \Delta_T + ({}^w R_c(T_{c,1}) - {}^w R_c(T_{c,2})) {}^d t_c$, where $\kappa_d^{-1} {}^w R_c(T_{c,1}) {}^c R_d v_d \Delta_T$ and

$({}^w R_c(T_{c,1}) - {}^w R_c(T_{c,2})) {}^d t_c$ denote the updates brought by robot translation and rotation, respectively.

We compare the above estimated position-only trajectory against the ground-truth trajectory derived from the stereo camera's absolute-position measurements from the AprilTag board. Absolute Trajectory Error (ATE) and Relative Position Error (RPE) are selected as evaluation metrics. We evaluate five methods and compare their performance:

- **UIC**: our UIC initialization method in Algorithm 2.
- **BCD (init. 1)**: BCD initialized with manually measured extrinsic parameters.
- **BCD (init. 2)**: BCD initialized with ${}^d R_b = \mathbf{I}_3$, ${}^d t_b = 0$.
- **Manual w. δ_T** : use manually measured ${}^d R_b$ and ${}^d t_b$, and compensate for the clock offset estimated by UIC.
- **Manual w.o. δ_T** : use manually measured ${}^d R_b$ and ${}^d t_b$, with the clock offset fixed at 0.

We recorded three trajectories, denoted as A, B, and C. For each trajectory, we perform calibration on that dataset and

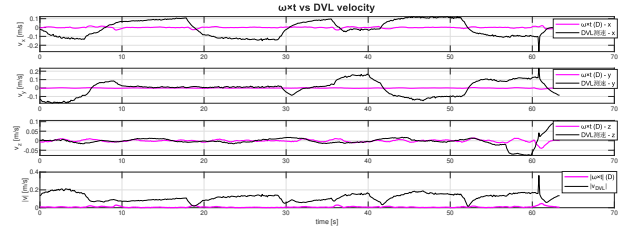


Fig. 6: DVL velocity vs. $\omega \times {}^d t_b$.

validate on the other two, yielding six calibration-validation pairs. The error results are summarized in TABLE I, and trajectories of each method are shown in Fig. 4. With good initial values, the BCD (init.1) method can achieve good performance. However, with poor initial values, BCD (init.2) method has the most unstable performance, showing the importance of a good initial value for the BCD algorithm. UIC method, which does not need initial values, obtains a similar or even better performance than the BCD method with good initial values and outperforms both manual methods. The small difference between the two manual methods suggests that the clock offset has a minor impact on calibration and the state estimation process.

We also analyze the performance with respect to the measurement number. We use 50, 110, 600, and 1300 measurements from trajectory B, respectively, to evaluate the performances of different methods. Fig. 5 shows that the performances of UIC and BCD (init. 1) improve as the measurement increases. The Manual w. δ_T baseline also benefits from more data, suggesting that the estimated clock offset becomes more accurate with additional measurements.

Limitations: Although the experiments validate the effectiveness of our calibration method, the lever arm ${}^b t_b$ is not reliably estimated. This limitation stems from our experimental constraints and robot configuration: to keep the AprilTag board within the stereo camera's field of view, we restricted large rotational maneuvers. Consequently, the angular velocities are small, yielding insufficient excitation for the $\omega \times {}^b t_b$ coupling, which renders the lever arm weakly observable. Fig. 6 plots the DVL velocity measurements together with the $\omega \times {}^b t_c$ term throughout trajectory A, indicating that the $\omega \times {}^b t_c$ term is negligibly small.

VII. CONCLUSION AND FUTURE WORK

In this paper, we formalized the DVL spatiotemporal calibration as an MAP problem and introduced a UIC method to solve it. UIC provides a comparable performance as BCD with a good initial value. However, without a good initial value, BCD is unstable and may result in large errors. Our numerical studies show that, with a large number of measurements and sufficiently rich angular-velocity excitation, our method obtains excellent accuracy, and its effectiveness is also validated in real-world experiments.

For future work, we plan to replace the fixed kernel with online kernel estimation to better describe the underwater robot motions. In addition, we aim to upgrade both the robot and the calibration fixtures (e.g., the AprilTag board) to enable larger rotational excitation and thereby improve lever-arm estimation performance. We also intend to explore the feasibility of fully online calibration.

REFERENCES

- [1] L. Zhao, M. Zhou, and B. Loose, "Tightly-coupled visual- dvl- inertial odometry for robot-based ice-water boundary exploration," in *2023 IEEE/RSJ International Conference on Intelligent Robots and Systems (IROS)*, 2023, pp. 7127–7134.
- [2] Y. Huang, P. Li, S. Yan, Y. Ou, Z. Wu, M. Tan, and J. Yu, "Tightly-coupled visual-dvl fusion for accurate localization of underwater robots," in *2023 IEEE/RSJ International Conference on Intelligent Robots and Systems (IROS)*, 2023, pp. 8090–8095.
- [3] S. Xu, K. Zhang, Z. Hong, Y. Liu, and S. Wang, "Diso: Direct imaging sonar odometry," in *2024 IEEE International Conference on Robotics and Automation (ICRA)*, 2024, pp. 8573–8579.
- [4] J. McConnell, F. Chen, and B. Englot, "Overhead image factors for underwater sonar-based slam," *IEEE Robotics and Automation Letters*, vol. 7, no. 2, pp. 4901–4908, 2022.
- [5] S. E. Webster, L. L. Whitcomb, and R. M. Eustice, "Preliminary results in decentralized estimation for single-beacon acoustic underwater navigation," in *Robotics: Science and Systems*, vol. 10, 2010.
- [6] S. Xu, T. Luczynski, J. S. Willners, Z. Hong, K. Zhang, Y. R. Petillot, and S. Wang, "Underwater visual acoustic slam with extrinsic calibration," in *2021 IEEE/RSJ International Conference on Intelligent Robots and Systems (IROS)*. IEEE, 2021, pp. 7647–7652.
- [7] E. Westman and M. Kaess, "Underwater apriltag slam and calibration for high precision robot localization," in *tech. rep.* Carnegie Mellon University Pittsburgh, PA, 2018.
- [8] B. Xu and Y. Guo, "A novel dvl calibration method based on robust invariant extended kalman filter," *IEEE Transactions on Vehicular Technology*, vol. 71, no. 9, pp. 9422–9434, 2022.
- [9] B. Xu, L. Wang, S. Li, and J. Zhang, "A novel calibration method of sins/dvl integration navigation system based on quaternion," *IEEE Sensors Journal*, vol. 20, no. 16, pp. 9567–9580, 2020.
- [10] S. Liu, T. Zhang, and Y. Zhu, "A gnss aided calibration method for dvl error based on the optimal-request," *IEEE Sensors Journal*, vol. 22, no. 22, pp. 21899–21910, 2022.
- [11] B. Wang, J. Liu, Z. Deng, and M. Fu, "A model-free calibration method of inertial navigation system and doppler sensors," *IEEE Sensors Journal*, vol. 21, no. 2, pp. 2219–2229, 2021.
- [12] T. Qin and S. Shen, "Online temporal calibration for monocular visual-inertial systems," in *2018 IEEE/RSJ International Conference on Intelligent Robots and Systems (IROS)*. IEEE, 2018, pp. 3662–3669.
- [13] J. Rehder, R. Siegwart, and P. Furgale, "A general approach to spatiotemporal calibration in multisensor systems," *IEEE Transactions on Robotics*, vol. 32, no. 2, pp. 383–398, 2016.
- [14] P. Furgale, J. Rehder, and R. Siegwart, "Unified temporal and spatial calibration for multi-sensor systems," in *2013 IEEE/RSJ International Conference on Intelligent Robots and Systems*, 2013, pp. 1280–1286.
- [15] J. Peršić, L. Petrović, I. Marković, and I. Petrović, "Spatiotemporal multisensor calibration via gaussian processes moving target tracking," *IEEE Transactions on Robotics*, vol. 37, no. 5, pp. 1401–1415, 2021.
- [16] R. Hartley, M. Ghaffari, R. M. Eustice, and J. W. Grizzle, "Contact-aided invariant extended kalman filtering for robot state estimation," *The International Journal of Robotics Research*, vol. 39, no. 4, pp. 402–430, 2020.
- [17] F. Dellaert, "Factor graphs and gtsam: A hands-on introduction," *Georgia Institute of Technology, Tech. Rep.*, vol. 2, no. 4, 2012.
- [18] C. H. Tong, P. Furgale, and T. D. Barfoot, "Gaussian process gauss-newton for non-parametric simultaneous localization and mapping," *The International Journal of Robotics Research*, vol. 32, no. 5, pp. 507–525, 2013. [Online]. Available: <https://doi.org/10.1177/0278364913478672>
- [19] C. K. Williams and C. E. Rasmussen, *Gaussian processes for machine learning*. MIT press Cambridge, MA, 2006, vol. 2, no. 3.
- [20] A. Wald, "The fitting of straight lines if both variables are subject to error," *The annals of mathematical statistics*, vol. 11, no. 3, pp. 284–300, 1940.
- [21] B.-Q. Mu and H.-F. Chen, "Recursive identification of multi-input multi-output errors-in-variables hammerstein systems," *IEEE Transactions on Automatic Control*, vol. 60, no. 3, pp. 843–849, 2014.
- [22] O. Reiersøl, "Identifiability of a linear relation between variables which are subject to error," *Econometrica: Journal of the Econometric Society*, pp. 375–389, 1950.
- [23] B. Mu, E.-W. Bai, W. X. Zheng, and Q. Zhu, "A globally consistent nonlinear least squares estimator for identification of nonlinear rational systems," *Automatica*, vol. 77, pp. 322–335, 2017.
- [24] T. Y. Tang, D. J. Yoon, and T. D. Barfoot, "A white-noise-on-jerk motion prior for continuous-time trajectory estimation on $se(3)$," *IEEE Robotics and Automation Letters*, vol. 4, no. 2, pp. 594–601, 2019.